Progress In Electromagnetics Research, Vol. 150, 163–182, 2015

Recent Advances in the Asymptotic Theory of Diffraction by Elongated Bodies

Ivan V. Andronov[1] and Raj Mittra[2, *]

(*Invited Paper*)

Abstract—The asymptotic approach to the problem of high-frequency diffraction by elongated bodies is discussed in this work. The classical expansion is shown to require the frequencies to be too high for it to be applicable. Attempts to improve the approximating properties of the asymptotic methods are discussed. It is shown that effective approximations appear under the supposition that the squared transverse dimension of the body is proportional to its longitudinal size measured in wavelengths. This is referred to herein as the case of strongly elongated body and is examined in detail. It is assumed that the body has a rotational symmetry and can be well approximated by a spheroid. The cases of axial incidence and that of incidence at a grazing angle to the axis are considered. Both the asymptotics of the induced currents on the surface and of the far field amplitude are developed. Comparison with numerical results for a set of test problems shows that the leading terms of the new asymptotics provide good approximation in a uniform manner with respect to the rate of elongation. Some effects typical for scattering by elongated bodies are discussed.

1. INTRODUCTION

Interest in high-frequency diffraction developed many years ago to fulfill the needs of numerous applications in radioengineering. Since computers were not powerful at that time, alternatives to purely numerical analysis were highly appreciated. Methods of high-frequency diffraction remain an important tool for the analysis of wave phenomena even today. Classical results of Fock, Keller and others are restricted to geometries in which there is a single large parameter $k\rho$, which measures the characteristic size in wavelengths. The condition of validity of these asymptotic expansions requires that all other quantities describing the problem not compete with this large parameter. In some cases, this imposes conditions that are too restrictive on the frequency, because they require the frequency to be very high. One such case is the diffraction by elongated bodies.

It is worth noting that purely numerical methods may fail if the body is sufficiently large, and this often prompts us to use high-frequency asymptotics or hybrid methods. However, if the body is highly elongated, there may be a gap between frequencies at which numerical methods work and those for which asymptotic approaches are viable. New asymptotic formulas, presented herein, aim to close this gap.

To render the Maxwell's equations symmetric we introduce the vectors $\mathbf{E}$ and $\mathbf{H}$, where $\mathbf{E}$ is electric vector divided by characteristic impedance of the space $\sqrt{\mu/\varepsilon}$ and $\mathbf{H}$ is magnetic vector. We assume that the time factor omitted thorough out the paper is $e^{-i\omega t}$. When dealing with general formulas valid both for TE and TM waves as well as for scalar acoustic waves we shall denote the field by U.

Received 14 January 2015, Accepted 26 February 2015, Scheduled 1 March 2015

* Corresponding author: Raj Mittra (rajmittra@ieee.org).

[1] Department of Computational Physics, St. Petersburg State University, Ulianovskaya 1-1, Petrodvoters 198504, Russia.

[2] Electromagnetic Communication Lab, EE Department, Pennsylvania State University, 319 Electrical Engineering East University Park, PA 16802-2705, USA.

First, we remind the reader of the key issues of classical Fock asymptotics and describe the attempts to improve the applicability of these asymptotics. Then, in Section 4, we discuss the recently proposed asymptotic approach to the problems of diffraction by strongly elongated bodies. We present only the leading order terms, and discuss their approximating properties by comparing asymptotic and numerical results in Section 5.

2. FOCK ASYMPTOTICS

For elongated body, the problem possesses another large parameter Λ besides the usual asymptotically large parameter $k\rho$. The latter can be defined as the ratio of surface curvatures ρ/ρ_t, or the ratio of the length of the body to its transverse dimensions.

If the frequency is very high then $\Lambda \ll k\rho$, and the classical asymptotic results [1] are applicable. We remind the reader that the asymptotics of the fields in the vicinity of the light-shadow boundary on the surface of a convex body have been extensively developed in the past. This so-called Fock domain appears to be the cradle of creeping waves which propagate to the shadow region of the boundary, and of the Fresnel transition field in the penumbra region.

Our first step is to introduce a coordinate system in which the surface of the body coincides with one of the coordinates surfaces. Usually such a coordinate system is formed by adding the normal to the semi-geodesic coordinates on the surface. That is, we consider a set of geodesics whose directions are defined by the rays of the incident field, and measure the first coordinate s along these geodesics starting from a reference line, which is usually the light-shadow boundary on the surface. The second surface coordinate t just parameterizes the geodesics from this set. In this approach, the way how the normal coordinate is defined is not important, and it can be taken as the geometrical distance to the surface. However, when dealing with elongated bodies at frequencies that are not too high we will return to this question and choose the normal coordinate differently. Once the coordinate system has been introduced, all the equations and the boundary conditions of the problem should be rewritten in this coordinate system. The characteristics of the surface and the incident field, such as radius of curvature ρ of the geodesics, their divergence, radius of transverse curvature ρ_t and the torsion appear in the above equations.

The next step in the asymptotic procedure is to choose the scales of the coordinates. One should scale the coordinates in a way such that the derivatives of the field by the scaled coordinates can be considered as quantities that are on the order of unity. In our case, the field depends on s in the form of a dominant factor e^{iks}, multiplied by a slower varying function called the attenuation function

$$U = \exp(iks)u(s,n). \tag{1}$$

We substitute the above representation into the equation and rewrite it in terms of the coordinates $(s,\, n)$ as

$$2ik\frac{\partial u}{\partial s} + \frac{\partial^2 u}{\partial s^2} + \frac{n}{\rho+n}\frac{\rho'}{\rho}\left(iku + \frac{\partial u}{\partial n}\right) + \frac{\partial^2 u}{\partial n^2} + 2\frac{n}{\rho}\frac{\partial^2 u}{\partial n^2} + \frac{n^2}{\rho^2}\frac{\partial^2 u}{\partial n^2} + \frac{1}{\rho}\frac{\partial u}{\partial n} + \frac{n}{\rho^2}\frac{\partial u}{\partial n} + 2k^2\frac{n}{\rho}u + k^2\frac{n^2}{\rho^2}u + \ldots = 0. \tag{2}$$

In (2) the dots denote higher order terms which will be omitted in our analysis.

Next, we choose the principal-order terms in this equation by introducing the stretched coordinates $k^\alpha s$, $k^\beta n$, where the exponents α and β are unknowns as yet. We assume that differentiation by the stretched coordinates does not change the order of these terms. Since u does not vary with s faster than the exponential factor in (1), $\alpha < 1$. This enables us to consider $\partial^2 u/\partial s^2$ as a correction to the term $2ik\partial u/\partial s$ and, therefore, we exclude it from the set of principal-order terms. Furthermore, to be able to set the boundary condition at $n = 0$, and the radiation condition at $n = +\infty$, the second-order derivative with respect to n should be included in the set of the principal-order terms. This implies that $\beta > 0$ and the terms with $\partial u/\partial n$ are smaller than $\partial^2 u/\partial n^2$. Finally, the n^2 terms are smaller than similar terms with the first power of n. In view of this, the following three terms may be considered to be the principal terms in Equation (2): $\frac{\partial^2 u}{\partial n^2}$, $2ik\frac{\partial u}{\partial s}$ and $2k^2\frac{n}{\rho}u$. Preserving all three terms yields the well known Leontovich parabolic equation:

$$2ik\frac{\partial u}{\partial s} + \frac{\partial^2 u}{\partial n^2} + 2k^2\frac{n}{\rho}u = 0. \tag{3}$$

Simultaneously, we have determined the size of the Fock domain. Parabolic Equation (3) fixes the scales $\alpha = 1/3$ and $\beta = 2/3$. Thus, the Fock domain is as small as $k^{-1/3}$ along the surface, and as small as $k^{-2/3}$ in the direction of the normal. Within such a small domain any general surface is almost cylindrical, which explains why derivatives with respect to the second surface coordinate t are not included in the parabolic equation. Moreover, in the Fock domain, we can usually replace $\rho(s,t)$ by its value $\rho_0(t) = \rho(0,t)$. Then the coefficients of the parabolic equation become constant, and by introducing the boundary-layer coordinates

$$\sigma = m\frac{s}{\rho_0}, \quad \nu = 2m^2\frac{n}{\rho_0}, \quad m = \left(\frac{k\rho_0}{2}\right)^{1/3}, \tag{4}$$

we can rewrite (3) in its simplest form

$$\frac{\partial^2 u}{\partial \nu^2} + i\frac{\partial u}{\partial \sigma} + \nu u = 0. \tag{5}$$

We solve the above equation via the use of Fourier transform to get:

$$u = \int_{-\infty}^{+\infty} e^{i\sigma\zeta} c(\zeta)\Big(v(\zeta-\nu) + R(\zeta)w_1(\zeta-\nu)\Big)d\zeta. \tag{6}$$

Here v and w_1 are the Airy functions in Fock notation. The part of the solution which contains the Airy function $v(\zeta-\nu)$ corresponds to the incident field while the part of the solution which contains the Airy function $w_1(\zeta-\nu)$ represents the secondary field. The function w_1 is chosen to satisfy the radiation condition. The coefficient R is determined from the boundary condition. Thus from the Neumann condition, for the TM polarization we find

$$R^{\mathrm{TM}}(\zeta) = -\frac{\dot{v}(\zeta)}{\dot{w}_1(\zeta)}, \tag{7}$$

where dot denotes the derivative. For the TE polarization, by imposing the Dirichlet condition we find that

$$R^{\mathrm{TE}}(\zeta) = -\frac{v(\zeta)}{w_1(\zeta)}. \tag{8}$$

The amplitude $c(\zeta)$ remains undetermined as yet, and it enables us to match the local asymptotics in the Fock domain to the incident field. For this purpose we consider the incident wave and represent it in the stretched coordinates (σ,ν) of the boundary layer. For example, for the case of an incident plane wave we have

$$u^i = u^i(C)\exp\left\{i\left(\sigma\nu - \frac{1}{3}\sigma^3\right)\right\}.$$

By inserting this expression in (6), we obtain the integral equation for the amplitude $c(\zeta)$, which reads

$$\int_{-\infty}^{+\infty} e^{i\sigma\zeta} c(\zeta)v(\zeta-\nu)d\zeta = u^i(C)\exp\left\{i\left(\sigma\nu - \frac{1}{3}\sigma^3\right)\right\}. \tag{9}$$

Applying the Fourier transform we find

$$c(\zeta) = u^i(C)\frac{1}{\sqrt{\pi}}.$$

If we take the observation point on the surface in the Formula (6), i.e., if we let $\nu = 0$, we obtain the well-known expression for the field associated with the TE-polarized wave, viz.,

$$E = U^i(C)\frac{e^{iks}}{\sqrt{\pi}}\int_{-\infty}^{+\infty} e^{i\sigma\zeta}\frac{d\zeta}{w_1(\zeta)}. \tag{10}$$

Similarly, for the induced current of the TM wave, we get

$$J = U^i(C)\frac{e^{iks}}{\sqrt{\pi}}\int_{-\infty}^{+\infty} e^{i\sigma\zeta}\frac{d\zeta}{\dot{w}_1(\zeta)}. \tag{11}$$

Although (10) and (11) only contain the leading order terms of the asymptotics, and the asymptotic decomposition is carried out by using the inverse powers of m, i.e., fractional powers of $k\rho$, they yield a rather accurate approximation for the field even when the frequency is not too high. We can verify this from Figure 1 taken from [2] (the original is in [3]), where the currents induced on a circular cylinder, whose diameter is equal to the wavelength, have been presented. It is worthwhile to point out that in the diffraction problem the current is formed by the interference of two waves. One travels in the clockwise direction from the light-shadow boundary, while the other originates from the light-shadow boundary on the opposite side of the cylinder and travels in the counter-clockwise direction. Both of these waves are attenuated, but as the diameter of the cylinder is not large, the wave which encircles the shadowed side does not travel a large distance, and its contribution remains noticeable in the form of the oscillations of the field amplitude.

Since the second surface coordinate t is not involved in the higher-order operator, the leading-order term of the asymptotics is not affected by the transverse curvature of the body. However the induced currents are different if the body is not a cylinder, but a sphere, and the agreement between the real currents and the asymptotics is not as good in this case as it is for the case of the cylinder. The comparison with the numerical results presented in [4, 5] show that for the sphere with $k\rho = 10$ the accuracy of the asymptotic formulas is about 15–20% and for prolate spheroids the accuracy of the asymptotics is much lower. Attempts to improve the situation entail the computation of the next-order terms of the asymptotics, and we mention here only two previous works that have attempted to do this. The first one is by Hong [6], who has derived the second-order term of the asymptotics, both for the fields in the Fock domain and for creeping waves in the deep shadow. He has considered an arbitrary (with some inessential restrictions) smooth convex surface with ideal boundary conditions. For the case of a sphere, it was possible to find not only the second-order term, but the entire series representation [7]. However, the latter result differs by a factor of 2 from the one by Hong. In spite of the possibility of using the second- and higher-order terms, the lower bound of frequency domain where the asymptotic formulas yield sufficiently accurate representations for the currents on the sphere, have remained almost unchanged. This leads us to conclude that the higher-order terms do not enlarge the domain of applicability of the first-order representation.

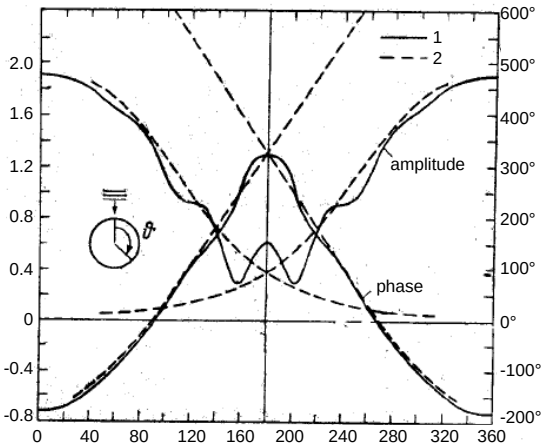

Figure 1. Currents on a perfectly conducting circular cylinder with the diameter equal to the wavelength. Solid line — exact, dashed — Fock asymptotics (11).

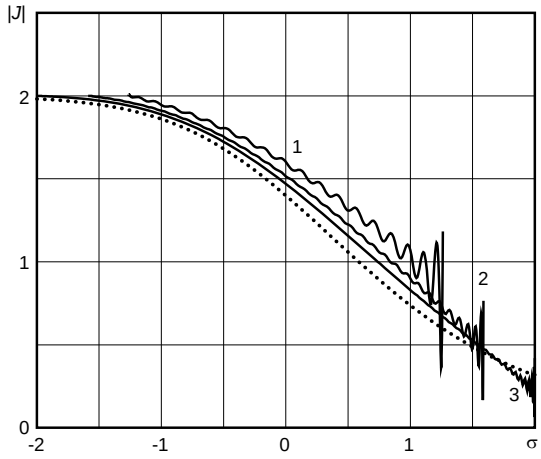

Figure 2. Induced current amplitude on the spheroid with semiaxes $b = 1.25\,\mathrm{m}$, $a = 0.5\,\mathrm{m}$ at frequencies 1, 2 and 4 GHz (curves 1, 2, 3) and the asymptotic approximation by Fock (dotted curve).

3. MODERATELY ELONGATED BODIES

For elongated objects, such as spheroids, the lower frequency bound of the domain where Fock formulas can be used shifts to $kb > 100$ and larger. We can deduce this by comparing the principal-order term of the asymptotics with numerical results. Figure 2 presents the induced currents on the spheroid with semiaxes $a = 0.5\,\mathrm{m}$ and $b = 1.25\,\mathrm{m}$, at frequencies 1, 2 and 4 GHz and the asymptotics (11). We use the stretched coordinate σ in which the "size" of the spheroid changes with frequency, but the asymptotic approximation remains unchanged. (More results can be found in [8]). Figure 2 shows that the Fock formula underestimates the values for the currents. This is consistent with the observation that the edges or surfaces with high transverse curvature decrease the attenuation of the creeping waves. That is, large transverse curvature or sharp edges promote the propagation of waves, as exemplified by the following cases. While studying diffraction by disks Senior [9] observed, in 1969, that a wave propagates with low attenuation along the rim of the disk. The Sommerfeld wave [10] propagates with only a logarithmic attenuation along conducting wires. Finally, a source on a cylinder excites a wave that propagates along the generatrix of the cylinder, and only decreases as the inverse of the square root of the distance [11].

The impact of transverse curvature on the propagation constant of creeping waves, and more specifically, the case of creeping wave on elongated bodies, has been analyzed in [12] (see also [13]). In the spirit of the work of Engineer et al. [14], who have studied the problem of diffraction by 2D slender bodies, it was assumed that besides the usual asymptotic parameter $k\rho$, the geometrical characteristics of the body form another large parameter $\Lambda = \rho/\rho_t$, with which the asymptotic parameter may compete. Analysis of the scales shows that reorganization of the usual creeping waves asymptotics as well as the asymptotics in Fock domain takes place when Λ reaches the order of m, i.e., becomes as large as $(k\rho)^{1/3}$. This case was referred to in [12] as the case of *moderately elongated body*.

In this case, as shown in [13], one can introduce the effective impedance

$$Z = \frac{i}{2k\rho_t} \tag{12}$$

to account for the effects of high transverse curvature. However, the approach for moderately elongated bodies still results in an underestimation of the currents.

The *strongly elongated body* was defined in [12] as the body in which the transverse curvature $1/\rho_t$ is on the order of $k^{2/3}\rho^{-1/3}$, implying that $\Lambda \sim m^2$. The approach given in [12], however, is not as accurate as we desire and we will now describe a different method in the rest of the paper.

4. DIFFRACTION BY A STRONGLY ELONGATED BODY

As explained above, we assume that besides the large asymptotic parameter $k\rho$, the problem of diffraction possesses another large parameter $\Lambda = \rho/\rho_t$ such that $\Lambda \sim (k\rho)^{2/3}$. If for such a problem we maintain the same orders that define the size of Fock domain, then the entire strongly-elongated body will be contained inside it, and this poses some difficulties. First of all, the field loses locality with respect to the transverse coordinate and we are forced to consider only rotationally symmetric bodies. Secondly, the radius of curvature ρ cannot be assumed to be constant as it can be in the classical case, and its dependence on the surface coordinate should be taken into account. This second difficulty is overcome by assuming that the body can be well approximated with an appropriately chosen spheroid.

4.1. Boundary Layer, Scales and Coordinates

Let the elongated body possess the symmetry of revolution and let ρ and ρ_t be its main radii of curvature at the widest cross-section. We assume that the body is spheroid-like, i.e., its surface deviates from the surface of the spheroid by an asymptotically small distance. The radii of curvature define the semiaxes of this spheroid as

$$a = \rho_t, \quad b = \sqrt{\rho\rho_t}. \tag{13}$$

The assumption that the body be strongly elongated in terms of the semiaxes can be expressed as

$$\chi \equiv \frac{ka^2}{b} = O(1). \tag{14}$$

The parameter χ is referred to as the elongation parameter. We use the spheroidal coordinates (ξ, η, φ) related to the cylindrical (r, z, φ) ones via the formulas

$$z = p\xi\eta, \quad r = p\sqrt{\xi^2 - 1}\sqrt{1 - \eta^2}, \tag{15}$$

where $p = \sqrt{b^2 - a^2}$ is the half-focal distance and the z axis is the axis of the body.

For strongly elongated spheroids, the radial coordinate ξ is close to one in the boundary layer near the surface. Thus, it is convenient to replace ξ with another coordinate, which we denote by τ. We introduce such a coordinate by using the formula

$$\tau = 2\chi^{-1}kb(\xi - 1), \tag{16}$$

so that $\tau = 0$ on the axis and it equals 1 on the surface. The coordinates (η, τ) serve as the coordinates of the boundary layer, η replaces the surface coordinate σ and τ replaces the normal coordinate ν of the Fock asymptotics.

Keeping in mind that $a \ll b$, we can simplify the formulas for the boundary-layer coordinates to

$$\begin{cases} r = a\sqrt{1 - \eta^2}\sqrt{\tau}, \\ z = b\eta + \dfrac{a^2}{2b}(\tau - 1)\eta. \end{cases} \tag{17}$$

This change does not influence the asymptotic procedure which pertains to the leading order, although may affect the higher-order corrections, which we ignore however.

For an ordinary (not elongated) body, the use of the parabolic equation method suggests that the factor e^{iks} be separated. Computing the arc-length s on the spheroid is not an easy task; however, we can use a simpler factor $e^{ikp\eta}$ or $e^{ikb\eta}$ if we again exploit the fact that $a \ll b$. These factors agree with e^{iks} up to the terms on the order of unity, and we can choose any of them. The formulas become a little more compact if we choose $e^{ikp\eta}$ instead, and we simplify it to

$$\exp\left(ikb\eta - \frac{i}{2}\chi\eta\right). \tag{18}$$

Once we have chosen the coordinates and the factor mentioned above, we can go ahead and generalize the problem, by allowing the wave to be incident at an angle with respect to the axis. However, the angle should be small, such that the phase shift corresponding to the trajectory of the wave along the geodesics on the surface differs from the phase shift of the multiplier (18) by no more than a quantity on the order of unity, implying that the angle of incidence ϑ should be such that

$$\beta \equiv \sqrt{kb}\vartheta = O(1). \tag{19}$$

Dimensionless quantities χ and β, that are on the order of unity, are the parameters of the asymptotic formulas, which we will derive below.

4.2. Integral Representation of the Field

We search for the solution of Maxwell's equations in the form of a Fourier series in terms of the angle φ. For the part of the electromagnetic field which depends on the angle in the form $e^{i\ell\varphi}$, we express all the components of electric and magnetic vectors via the E_φ and H_φ components. Below we denote the Fourier harmonics of these components as E_ℓ and H_ℓ. The functions E_ℓ and H_ℓ are solutions of the system of differential equations, which is cumbersome to handle, although it is standard in spheroidal coordinates. Separation of variables is possible only if $\ell = 0$ [15], and it leads to a representation of the field that utilizes spheroidal functions.

We now extract the dominant factor in (18), and neglect the lower-order terms by the asymptotic parameter kb. For the leading order, we obtain a system of parabolic equations. It can be easily split into two independent sets of equations for the new unknowns:

$$P_\ell(\tau, \eta) = \frac{E_\ell + iH_\ell}{2}, \quad Q_\ell(\tau, \eta) = \frac{E_\ell - iH_\ell}{2}. \tag{20}$$

These unknowns satisfy the equations

$$L_{\ell-1}P_\ell = 0, \quad L_{\ell+1}Q_\ell = 0, \tag{21}$$

where

$$L_n = \tau\frac{\partial^2}{\partial\tau^2} + \frac{\partial}{\partial\tau} + \frac{i\chi}{2}\left(1-\eta^2\right)\frac{\partial}{\partial\eta} + \frac{1}{4}\left(\chi^2\tau - \frac{n^2}{\tau} - \chi^2\left(1-\eta^2\right)\right). \tag{22}$$

The differential equations in (21) are considered together with the boundary conditions. For the case of a perfectly conducting surface, the boundary conditions require that the tangential components of the electric vector be zero on the surface, which leads to the conditions

$$P_\ell(1,\eta) + Q_\ell(1,\eta) = 0, \tag{23}$$

$$\frac{\partial P_\ell(1,\eta)}{\partial\tau} + \frac{1}{2}P_\ell(1,\eta) - \frac{\partial Q_\ell(1,\eta)}{\partial\tau} - \frac{1}{2}Q_\ell(1,\eta) = 0. \tag{24}$$

We also set the radiation conditions at infinity for the secondary field.

Parabolic operator (22) is amenable to a separation of variables. Elementary solution of the equation $L_nU = 0$ can be written in the form

$$U_n = \frac{1}{\sqrt{\tau}\sqrt{1-\eta^2}}\left(\frac{1-\eta}{1+\eta}\right)^{\mu} F_{\mu,n/2}\left(-i\chi\tau\right), \tag{25}$$

where $F_{\mu,n/2}(g)$ is a solution of the Whittaker equation [16]

$$F'' + \left(-\frac{1}{4} + \frac{\mu}{g} + \frac{1-n^2}{4g^2}\right)F = 0.$$

We choose the Whittaker functions $M_{\mu,n/2}(-i\chi\tau)$ to represent the incident field in (25). These functions are regular at $\tau = 0$, which results in solutions that are regular in the entire space. For the secondary field, we choose Whittaker functions $W_{\mu,n/2}(-i\chi\tau)$ which correspond to solutions satisfying the radiation condition in terms of τ.

We combine P_ℓ and Q_ℓ of the elementary solutions (25) in the form of integrals over the separation parameter μ (compare with representation (6) of Fock asymptotics) to get:

$$\begin{bmatrix} P_{\ell+1} \\ Q_{\ell-1} \end{bmatrix} = \frac{1}{\sqrt{\tau}\sqrt{1-\eta^2}}\int\left(\frac{1-\eta}{1+\eta}\right)^{\mu} c(\mu)\left(M_{\mu,\ell/2}\left(-i\chi\tau\right) + \begin{bmatrix} R^P_{\ell+1} \\ R^Q_{\ell-1} \end{bmatrix} W_{\mu,\ell/2}\left(-i\chi\tau\right)\right)d\mu.$$

In these representations we include the amplitude factors c and R that are dependent on μ. To define the path of integration, and the amplitude factors, we first consider the incident field below.

4.3. Representation of the Incident Field

An arbitrarily polarized plane electromagnetic wave can be represented as a sum of transverse electric (TE) and transverse magnetic (TM) waves. We define the transverse direction with respect to the plane of incidence and assume that it coincides with the XOZ plane in Cartesian coordinates. The plane of incidence is not defined for the axial case, but TE and TM waves can still be defined with respect to the plane XOZ.

Let us consider the TE case first. We set a unit amplitude for the incident TE wave and express its $\mathbf{E}$ and $\mathbf{H}$ fields as

$$\mathbf{E}^i = \exp\left(ikz\cos\vartheta + ikx\sin\vartheta\right)\mathbf{e}_y, \tag{26}$$

$$\mathbf{H}^i = \exp\left(ikz\cos\vartheta + ikx\sin\vartheta\right)\left\{-\cos\vartheta\mathbf{e}_x + \sin\vartheta\mathbf{e}_z\right\}, \tag{27}$$

where $\mathbf{e}_x$, $\mathbf{e}_y$ and $\mathbf{e}_z$ are the unit vectors of Cartesian coordinates. Next, we represent the incident wave in the form of a Fourier series as follows:

$$E^i_\varphi = \exp\left(ikz\cos\vartheta\right)\left\{iJ_1\left(kr\sin\vartheta\right) + \sum_{n=1}^{\infty} i^{n-1}\Big(J_{n-1}\left(kr\sin\vartheta\right) - J_{n+1}\left(kr\sin\vartheta\right)\Big)\cos(n\varphi)\right\}, \tag{28}$$

$$H^i_\varphi = \exp\left(ikz\cos\vartheta\right)\cos\vartheta\sum_{n=1}^{\infty} i^{n-1}\Big(J_{n-1}\left(kr\sin\vartheta\right) + J_{n+1}\left(kr\sin\vartheta\right)\Big)\sin(n\varphi). \tag{29}$$

Each of the harmonics of (28), (29) can be expanded in an asymptotic series in terms of inverse powers of kb. The leading order terms satisfy the parabolic Equation (21). Therefore the leading order terms in the asymptotic expansion of (28), (29) can be represented as a combination of elementary solutions (25) in which, as explained above, we should include the Whittaker function $M_{\mu,n/2}(-i\chi\tau)$. The problem of finding the leading-order representation of the incident wave as a combination of the elementary solutions (25) reduces to that of finding such a representation for the functions

$$\exp(ikz\cos\vartheta)\, J_n(kr\sin\vartheta).$$

When substituting here the expressions for the coordinates r and z we replace the trigonometric functions of small ϑ by their approximations: $\sin\vartheta \approx \vartheta$ and $\cos\vartheta \approx 1-\frac{1}{2}\vartheta^2$. By doing this, we obtain the equation

$$\frac{1}{\sqrt{\tau}\sqrt{1-\eta^2}} \int \left(\frac{1-\eta}{1+\eta}\right)^{\mu} A_n(\mu) M_{\mu,n/2}(-i\chi\tau) d\mu == V(\eta,\tau). \tag{30}$$

Both the left-hand as well as the right-hand side of this equation satisfy the parabolic equation with operator L_n. Therefore, if we find the amplitude $A_n(\mu)$ for any fixed τ, it will satisfy (30) for all other values of τ. This important property simplifies the problem of finding the solution. First, we rewrite (30) in the form

$$\frac{1}{\sqrt{\chi\tau}\beta\sqrt{1-\eta^2}} \int \left(\frac{1-\eta}{1+\eta}\right)^{\mu} \Omega_n(\mu) M_{\mu,n/2}\left(i\beta^2\right) M_{\mu,n/2}\left(-i\chi\tau\right) d\mu = V(\eta,\tau), \tag{31}$$

where

$$A_n(\mu) = \frac{M_{\mu,n/2}\left(-i\beta^2\right)}{\sqrt{\chi}\beta} \Omega_n(\mu). \tag{32}$$

We note that τ is presented in (31) only as the product $\chi\tau$. Thus, since Ω_n does not depend on τ, it does not depend on χ either. Further more; since $\chi\tau$ and $-\beta^2$ presented in (31) are symmetric, Ω_n does not depend on β either. This enables us to find Ω_n for any chosen $\chi\tau$ and β. Equation (31) takes the simplest form if β and $\chi\tau$ both $\to 0$. Computing this limit and using the asymptotics

$$\begin{aligned} M_{\mu,n/2}(g) &\sim g^{(1+n)/2}, \quad g \to 0, \\ J_n(g) &\sim \frac{1}{n!}\left(\frac{g}{2}\right)^n, \quad g \to 0 \end{aligned} \tag{33}$$

we reduce Equation (31) to

$$\int \left(\frac{1-\eta}{1+\eta}\right)^{\mu} \Omega_n(\mu) d\mu = \frac{1}{2^n n!}\left(1-\eta^2\right)^{(n+1)/2}. \tag{34}$$

We note that we have not yet chosen the path of integration. If we choose it now as the imaginary axis and set

$$\eta = \frac{s-1}{s+1},$$

Equation (34) reduces to

$$\int_{-i\infty}^{+i\infty} s^{-\mu} \Omega_n(\mu) d\mu = \frac{2}{n!}\left(\frac{\sqrt{s}}{s+1}\right)^{n+1}.$$

We identify the left-hand side of this equation with inverse Mellin transform and find

$$\Omega_n(\mu) = \frac{1}{\pi(n!)^2}\Gamma\left(\frac{n+1}{2}+\mu\right)\Gamma\left(\frac{n+1}{2}-\mu\right). \tag{35}$$

Using (35) and changing the integration variable to $t = -i\mu$ we can write the incident plane TE wave in the form:

$$\begin{aligned} E^i_{\varphi} = -i\frac{\exp(ikb\eta - i\chi\eta/2)}{\sqrt{1-\eta^2}\beta\sqrt{\chi\tau}} \int_{-\infty}^{+\infty} \left(\frac{1-\eta}{1+\eta}\right)^{it} \Bigg\{ -\Omega_1(it) M_{it,\frac{1}{2}}(-i\chi\tau) M_{it,1/2}(i\beta^2) \\ + \sum_{\ell=1}^{+\infty} i^{\ell}\cos(\ell\varphi)\Big[\Omega_{\ell-1}(it) M_{it,\frac{\ell-1}{2}}\left(-i\chi\tau\right) M_{it,\frac{\ell-1}{2}}\left(i\beta^2\right) - \Omega_{\ell+1}(it) M_{it,\frac{\ell+1}{2}}(-i\chi\tau) M_{it,\frac{\ell+1}{2}}\left(i\beta^2\right)\Big]\Bigg\} dt, \end{aligned} \tag{36}$$

$$H_\varphi^i = -i\frac{\exp(ikb\eta - i\chi\eta/2)}{\sqrt{1-\eta^2}\beta\sqrt{\chi\tau}}\int\limits_{-\infty}^{+\infty}\left(\frac{1-\eta}{1+\eta}\right)^{it}\sum_{\ell=1}^{+\infty} i^\ell \sin(\ell\varphi)\left[\Omega_{\ell-1}(it)M_{it,\frac{\ell-1}{2}}(-i\chi\tau)M_{it,\frac{\ell-1}{2}}\left(i\beta^2\right)\right.$$
$$\left.+\Omega_{\ell+1}(it)M_{it,\frac{\ell+1}{2}}(-i\chi\tau)M_{it,\frac{\ell+1}{2}}(i\beta^2)\right]dt. \tag{37}$$

The representations for the TM plane wave

$$\mathbf{E}^i = \exp\left(ikz\cos\vartheta + ikx\sin\vartheta\right)\left\{\cos\vartheta\mathbf{e}_x - \sin\vartheta\mathbf{e}_z\right\},$$
$$\mathbf{H}^i = \exp\left(ikz\cos\vartheta + ikx\sin\vartheta\right)\mathbf{e}_y$$

can be derived analogously. The electric field is given by the expression (37) and the magnetic field can be expressed as in (36) with the opposite sign.

4.4. Boundary Conditions and the Induced Currents

The representations for the secondary fields are similar to (36) and (37), the only change being the replacement of Whittaker functions $M_{it,n}(-i\chi\tau)$ with the functions $W_{it,n}(-i\chi\tau)$. Note that the Whittaker functions $W_{it,n}(-i\chi\tau)$ are chosen because they satisfy the radiation condition. For the TE case we have, in accordance with (20) and (21),

$$E_\varphi^s = -i\frac{\exp(ikb\eta - i\chi\eta/2)}{\sqrt{1-\eta^2}\beta\sqrt{\chi\tau}}\int\limits_{-\infty}^{+\infty}\left(\frac{1-\eta}{1+\eta}\right)^{it}\left\{-\Omega_1(it)T_0(t)W_{it,\frac{1}{2}}(-i\chi\tau)M_{it,\frac{1}{2}}\left(i\beta^2\right) + \sum_{\ell=1}^{+\infty} i^\ell\cos(\ell\varphi)\right.$$
$$\left.\times\left[\Omega_{\ell-1}(it)R_\ell(t)W_{it,\frac{\ell-1}{2}}(-i\chi\tau)M_{it,\frac{\ell-1}{2}}\left(i\beta^2\right) - \Omega_{\ell+1}(it)T_\ell(t)W_{it,\frac{\ell+1}{2}}(-i\chi\tau)M_{it,\frac{\ell+1}{2}}\left(i\beta^2\right)\right]\right\}dt, \tag{38}$$

$$H_\varphi^s = -i\frac{\exp(ikb\eta - i\chi\eta/2)}{\sqrt{1-\eta^2}\beta\sqrt{\chi\tau}}\int\limits_{-\infty}^{+\infty}\left(\frac{1-\eta}{1+\eta}\right)^{it}\sum_{\ell=1}^{+\infty} i^\ell \sin(\ell\varphi)\left[\Omega_{\ell-1}(it)R_\ell(t)W_{it,\frac{\ell-1}{2}}(-i\chi\tau)M_{it,\frac{\ell-1}{2}}\left(i\beta^2\right)\right.$$
$$\left.+\Omega_{\ell+1}(it)T_\ell(t)W_{it,\frac{\ell+1}{2}}(-i\chi\tau)M_{it,\frac{\ell+1}{2}}\left(i\beta^2\right)\right]dt. \tag{39}$$

The functions $R_\ell(t)$ and $T_\ell(t)$, introduced herein, play the role of the reflection coefficients in some sense, and can be found when the sum of the incident and secondary fields is substituted in the boundary conditions (23) and (24). Evidently, each of the harmonics satisfies the boundary conditions separately. For the TE case, we find (for details of the derivations see [17]):

$$T_0 = -\frac{M_{it,1/2}(-i\chi)}{W_{it,1/2}(-i\chi)}, \tag{40}$$

$$[1mm]T_\ell = -\frac{Y_{\ell-1,\ell+1}}{Z_\ell} - \frac{1}{Z_\ell}\frac{\mathcal{W}_{(\ell-1)/2}}{C_\ell}, \quad R_\ell = -\frac{Y_{\ell+1,\ell-1}}{Z_\ell} - \frac{1}{Z_\ell}\mathcal{W}_{(\ell+1)/2}C_\ell, \quad \ell = 1,2,\ldots \tag{41}$$

where

$$C_\ell = \frac{\ell^2+4t}{2\ell^2(\ell+1)^2}\frac{M_{it,(\ell+1)/2}(i\beta^2)}{M_{it,(\ell-1)/2}(i\beta^2)},$$
$$Y_{n,m} = W_{it,\frac{n}{2}}(-i\chi)\dot{M}_{it,\frac{m}{2}}(-i\chi) + \dot{W}_{it,\frac{n}{2}}(-i\chi)M_{it,\frac{m}{2}}(-i\chi).$$
$$Z_n = W_{i\lambda,\frac{n-1}{2}}(-i\chi)\dot{W}_{i\lambda,\frac{n+1}{2}}(-i\chi) + \dot{W}_{i\lambda,\frac{n-1}{2}}(-i\chi)W_{i\lambda,\frac{n+1}{2}}(-i\chi)$$

and $\mathcal{W}_n$ is the Wronskian of Whittaker functions [16]

$$\mathcal{W}_n = \dot{M}_{it,n}(g)W_{it,n}(g) - M_{it,n}(g)\dot{W}_{it,n}(g) = \frac{\Gamma(1+2n)}{\Gamma(1/2+n-it)}. \tag{42}$$

For the TM case, the formulas are similar. For this case, E_φ is given by the right-hand side of (39) while H_φ is given by the right-hand side of (38), with the common multiplier (-1). The reflection coefficients in these two formulas are as follows:

$$T_0 = -\frac{\dot{M}_{it,1/2}(-i\chi)}{\dot{W}_{it,1/2}(-i\chi)} \tag{43}$$

and the other coefficients T_ℓ, $\ell = 1, 2, \ldots$ and coefficients R_ℓ are defined by Formula (41), but with $C_{\ell\pm1}$ replaced with $-C_{\ell\pm1}$.

The expressions given in (36) through (39) describe the electromagnetic fields in the boundary layer near the surface of the spheroid. In contrast to the classical Fock asymptotics, they do not have locality with respect to the transverse surface coordinate. Indeed, by restricting our analysis to the bodies of revolution we obtain the Fourier series in terms of the transverse angular coordinate φ. In other respects, the structure of these set of formulas has some similarity with the classical asymptotics of the field in the Fock domain. For example, the Fourier integral in ζ in the classical asymptotics is replaced by another integral transform which is reducible to the Mellin transform. The Airy function $v(\zeta-\nu)$, which represents the incident plane wave in (6), is replaced with the Whittaker function $M_{it,n}(-i\chi\tau)$, while the Airy function $w_1(\zeta-\nu)$ which represents the secondary wave outgoing from the surface is replaced with the Whittaker function $W_{it,n}(-i\chi\tau)$. The reflection coefficients (7) and (8) become more complex and are given by the expressions in (40), (41), and (43).

The induced current $\mathbf{J} = \mathbf{n}\times\mathbf{H}|_{\tau=1}$ can be found by using (36) through (39), with its principal component directed along η. After simple manipulations we can obtain

$$J_\eta = e^{ikb\eta}A(\eta,\chi,\beta,\varphi), \tag{44}$$

where, in the TE case $A = A^{\mathrm{TE}}$,

$$A^{\mathrm{TE}}(\eta,\chi,\beta,\varphi) = -\frac{2}{\pi}\frac{e^{-i\chi\eta/2}}{\sqrt{1-\eta^2}\sqrt{\chi}\beta}\int_{-\infty}^{+\infty}\left(\frac{1-\eta}{1+\eta}\right)^{it}\sum_{\ell=1}^{\infty}\frac{i^{\ell-1}\sin(\ell\varphi)}{(\ell+1)!Z_\ell}\left\{\Gamma\left(\frac{\ell}{2}+1+i\lambda\right)M_{it,\frac{\ell+1}{2}}(i\beta^2)W_{it,\frac{\ell-1}{2}}(-i\chi)\right.$$
$$\left.+\ell(\ell+1)\Gamma\left(\frac{\ell}{2}+it\right)M_{it,\frac{\ell-1}{2}}(i\beta^2)W_{it,\frac{\ell+1}{2}}(-i\chi)\right\}dt.$$

It is also convenient to represent the special function A^{TE} in terms of the Coulomb wave functions F and H^+ [16], and to use the program developed in [18] for their computation. Using the formulas

$$M_{it,\frac{\ell+1}{2}}(i\beta^2) = \frac{2ie^{i\pi\ell/4+\pi t/2}\Gamma(\ell+2)}{\sqrt{\Gamma(\ell/2+1+it)\Gamma(\ell/2+1-it)}}F_{\frac{\ell}{2}}\left(t,\frac{\beta^2}{2}\right),$$
$$W_{it,\frac{\ell-1}{2}}(-i\chi) = -ie^{i\pi\ell/4+\pi t/2}\sqrt{\frac{\Gamma(\ell/2+it)}{\Gamma(\ell/2-it)}}H^+_{\frac{\ell}{2}-1}\left(-t,\frac{\chi}{2}\right)$$

we obtain

$$A^{\mathrm{TE}} = \frac{-8e^{-i\chi\eta/2}}{\pi\sqrt{1-\eta^2}\sqrt{\chi}\beta}\int_{-\infty}^{+\infty}\left(\frac{1-\eta}{1+\eta}\right)^{it}\sum_{\ell=1}^{\infty}i^\ell\sin(\ell\varphi)\frac{F_{\frac{\ell}{2}}\left(t,\frac{\beta^2}{2}\right)H^+_{\frac{\ell-2}{2}}\left(-t,\frac{\chi}{2}\right)+F_{\frac{\ell-2}{2}}\left(t,\frac{\beta^2}{2}\right)H^+_{\frac{\ell}{2}}\left(-t,\frac{\chi}{2}\right)}{H^+_{\frac{\ell-2}{2}}\left(-t,\frac{\chi}{2}\right)\dot{H}^+_{\frac{\ell}{2}}\left(-t,\frac{\chi}{2}\right)+\dot{H}^+_{\frac{\ell-2}{2}}\left(-t,\frac{\chi}{2}\right)H^+_{\frac{\ell}{2}}\left(-t,\frac{\chi}{2}\right)}dt. \tag{45}$$

Similarly, for the TM case we can obtain

$$A^{\mathrm{TM}}(\eta,\chi,\beta,\varphi) = \frac{8e^{-i\chi\eta/2}}{\pi\sqrt{1-\eta^2}\sqrt{\chi}\beta}\int_{-\infty}^{+\infty}\left(\frac{1-\eta}{1+\eta}\right)^{it}\left\{\frac{1}{2}\frac{F_0\left(t,\frac{\beta^2}{2}\right)}{\dot{H}^+_0\left(-t,\frac{\chi}{2}\right)}+\sum_{\ell=1}^{\infty}i^\ell\cos(\ell\varphi)\right.$$
$$\left.\times\frac{F_{\frac{\ell}{2}}\left(t,\frac{\beta^2}{2}\right)H^+_{\frac{\ell-2}{2}}\left(-t,\frac{\chi}{2}\right)-F_{\frac{\ell-2}{2}}\left(t,\frac{\beta^2}{2}\right)H^+_{\frac{\ell}{2}}\left(-t,\frac{\chi}{2}\right)}{H^+_{\frac{\ell-2}{2}}\left(-t,\frac{\chi}{2}\right)\dot{H}^+_{\frac{\ell}{2}}\left(-t,\frac{\chi}{2}\right)+\dot{H}^+_{\frac{\ell-2}{2}}\left(-t,\frac{\chi}{2}\right)H^+_{\frac{\ell}{2}}\left(-t,\frac{\chi}{2}\right)}\right\}dt. \tag{46}$$

It is worth noting that for the case of axial incidence, one should consider the limit as $\beta \to 0$ in the above formulas. Only the Coulomb wave function $F_{\frac{-1}{2}}$ has a non-zero contribution in this case and the special functions A^{TE} and A^{TM} simplify to

$$A^{\mathrm{TE}}(\eta,\chi,0,\varphi) = A(\eta,\chi)\sin\varphi,$$
$$A^{\mathrm{TM}}(\eta,\chi,0,\varphi) = A(\eta,\chi)\cos\varphi,$$

where

$$A(\eta,\chi) = -\frac{4e^{-i\chi\eta/2}}{\sqrt{\pi\chi}\sqrt{1-\eta^2}} \int\limits_{-i\infty}^{+i\infty} \left(\frac{1-\eta}{1+\eta}\right)^{it} \frac{e^{-\pi t/2}}{\sqrt{\cosh(\pi t)}} \frac{H^+_{1/2}\left(-t,\frac{\chi}{2}\right)\, dt}{H^+_{-\frac{1}{2}}\left(-t,\frac{\chi}{2}\right)\dot{H}^+_{\frac{1}{2}}\left(-t,\frac{\chi}{2}\right) + \dot{H}^+_{-\frac{1}{2}}\left(-t,\frac{\chi}{2}\right)H^+_{\frac{1}{2}}\left(-t,\frac{\chi}{2}\right)}. \tag{47}$$

The expressions in (45), (46) and (47) are more cumbersome in comparison to the classical Fock function (11). However, with the help of the program from [18] their computations are relatively straightforward. The integrals converge quite rapidly and only a small interval contributes to the integral. As shown in [8] the function A reduces to the Fock function (11), when $\chi \to +\infty$.

4.5. Backward Wave

The total field in the boundary layer near the surface is the sum of the primary wave running in the positive direction of z together with waves that are formed when the primary wave encircles the ends of the spheroid. The asymptotics in (45) and (46) only describe the primary wave and are valid in the middle part of the spheroid. The reflected backward wave representation in the boundary layer can be written by noting that the backward wave runs in the opposite direction and that there is no incident backward wave. For the case of the axial incidence, considered in [19], the representation of the current corresponding to the backward wave is given by

$$J_b^{\mathrm{TE}} = e^{-ikb\eta}B(\eta,\chi)\sin\varphi, \quad J_b^{\mathrm{TM}} = e^{-ikb\eta}B(\eta,\chi)\cos\varphi,$$

where

$$B(\eta,\chi) = -\frac{4e^{i\chi\eta/2}}{\sqrt{\pi\chi}\sqrt{1-\eta^2}} \int\limits_{-i\infty}^{+i\infty} \left(\frac{1+\eta}{1-\eta}\right)^{it} \frac{e^{-\pi t/2}}{\sqrt{\cosh(\pi t)}} \frac{H^+_{1/2}\left(-t,\frac{\chi}{2}\right) r(t)dt}{H^+_{-\frac{1}{2}}\left(-t,\frac{\chi}{2}\right)\dot{H}^+_{\frac{1}{2}}\left(-t,\frac{\chi}{2}\right) + \dot{H}^+_{-\frac{1}{2}}\left(-t,\frac{\chi}{2}\right)H^+_{\frac{1}{2}}\left(-t,\frac{\chi}{2}\right)}. \tag{48}$$

The special function B is defined by the expression similar to the one given in (47) in which we change the sign of η and introduce an additional multiplier $r(t)$. The latter may be interpreted as the reflection coefficient from the tip of the spheroid. To find this multiplier one needs to construct the field in the vicinity of the spheroid tip, that is for $\eta \approx 1$, and match the sum $J + J_b$ with that field. The difficulty is that there is no asymptotic parameter in the region near the tip of the spheroid. Indeed, the radius of curvature of the surface at the tip is $\rho_e = a^2/b$. Therefore the parameter $k\rho_e$, which is equal to the elongation parameter χ, is on the order of unity. However, there is a way to circumvent this difficulty, as shown in [19], which is based on the observation that a very elongated ellipse is well-approximated by a parabola. Hence, if we replace the surface of the spheroid by the surface of the paraboloid defined by the equation

$$r^2 = 2\frac{a^2}{b}(b-z),$$

we can use the exact solution of Fock [20] to approximate the field. Matching this Fock solution to the sum of the forward and backward waves allows the reflection coefficient to be found

$$r(t) = ie^{2ikb-i\chi}\frac{\Gamma(1/2+it)}{\Gamma(1/2-it)}\sqrt{\frac{2t-i}{2t+i}}(4kb)^{-2it}. \tag{49}$$

We note that the asymptotic parameter kb is presented in (49) and, rigorously speaking, the formula requires further asymptotic simplifications in the process of computing the integral in (48), as the contribution of the residues in the zeros of the denominator

$$H^+_{-\frac{1}{2}}\left(-t,\frac{\chi}{2}\right)\dot{H}^+_{\frac{1}{2}}\left(-t,\frac{\chi}{2}\right) + \dot{H}^+_{-\frac{1}{2}}\left(-t,\frac{\chi}{2}\right)H^+_{\frac{1}{2}}\left(-t,\frac{\chi}{2}\right) = 0. \tag{50}$$

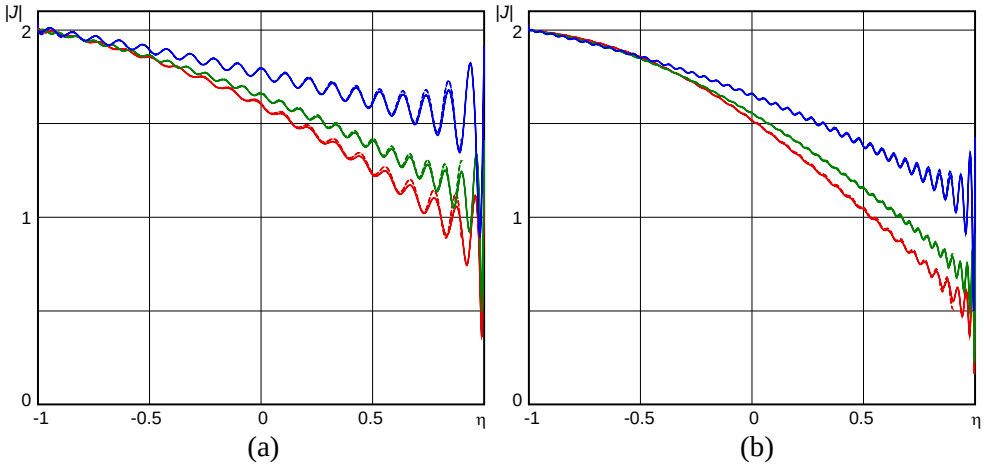

Figure 3. Amplitudes of the induced current on the spheroid No. 1 — red, No. 2 — green, No. 3 — blue (FEM — solid, asymptotics — dashed), (a) at 1 GHz and (b) at 2 GHz.

Table 1. Parameters of the test problems.

No.	a (m)	b (m)	at 1 GHz		at 2 GHz	
			χ	kb	χ	kb
1	0.5	1.25	4.19169	26.19806	8.38338	52.39613
2	0.5	1.76776695	2.96397	37.04966	5.92795	74.09931
3	0.3125	1.39754249	1.46452	29.29032	2.92903	58.58065

Solutions of Equation (50) lie in the lower complex half-plane of t (see [21] where solutions of (50) have been analyzed) and the main contribution to (48) is due to the residue in the pole with the maximal imaginary part of t. However, finding the solutions of the dispersion Equation (50) is not easy, and we compute the integral directly instead. Moreover, we expect that the formulas can also be applied in the case of values of kb, that are not too large, say $kb \approx 3$, when the approximation with one residue fails.

To illustrate the approximating nature of the asymptotic formulas we present in Figure 3 the results of the comparison in [19] of the currents induced by the axially incident plane wave on the surface of perfectly conducting spheroids. The trigonometric multiplier of φ is not considered. The results computed by the Finite Element Method (FEM) are plotted with solid curves and the asymptotic results are shown with dashed curves. The parameters of the test examples are presented in Table 1. We see that the agreement is quite good and it is slightly better for spheroids with larger elongations. This was expected, because the fact that a spheroid is strongly elongated was used when deriving the asymptotic formulas, in all of our derivations, and the terms that are small for elongated spheroids were neglected.

For $\vartheta \neq 0$, backward wave asymptotics can be found by using the same approach, but this has not been carried out as yet.

4.6. The Far Field Asymptotics

Since we have been able to obtain good approximations for the field in the boundary layer near the surface, the use of the Stratton-Chu formula in [22] enables us to derive the scattered fields. For perfectly conducting bodies this formula reduces to

$$\mathbf{H}^s(\mathbf{r}_0) = -\frac{1}{4\pi} \iint \mathbf{J}(\mathbf{r}) \times \nabla G(\mathbf{r}, \mathbf{r}_0) dS, \tag{51}$$

where $\mathbf{J}$ is the total induced current, $\times$ the vector product, G the scalar Green's function, and the integration is carried over the surface of the body.

Moving the observation point $\mathbf{r}_0$ in (51) to infinity along the ray, defined by the spherical coordinates ϑ_0 and φ_0, we compute the limit under the integration sign to obtain the formula for the far field amplitude of the magnetic field, which reads

$$\mathbf{\Psi} = -\frac{1}{4\pi}\iint \mathbf{J}\times\nabla\psi dS. \tag{52}$$

Here ψ is the far field amplitude of G. Its representation in the boundary layer near the surface can be found in [23]

$$\psi = \frac{1}{2}\psi_0 + \sum_{m=1}^{+\infty}\psi_m\cos[m(\varphi-\varphi_0)], \tag{53}$$

$$\psi_m = \frac{2i^{m+1}e^{-ikb\eta+i\chi\eta/2}}{\sqrt{1-\eta^2}\sqrt{\chi\tau}\beta_0}\int\limits_{-\infty}^{+\infty}\left(\frac{1+\eta}{1-\eta}\right)^{is} M_{is,\frac{m}{2}}(i\beta_0^2)\Omega_m(s)M_{is,\frac{m}{2}}(-i\chi\tau)ds, \tag{54}$$

where $\beta_0=\sqrt{kb}\vartheta_0$ is the scaled observation angle, and the amplitudes Ω_m are defined by (35).

Our goal is to find the leading order asymptotics of $\mathbf{\Psi}$. Towards this end, we substitute the asymptotics of the currents in (52). The approximations (38), (39) are not valid near the tips of the spheroid where focusing effects take place. Also, these formulas describe only the forward wave which runs from the illuminated domain to the shadow. Therefore, we can determine the far field only in those directions for which the main contribution to the integral in (52) arises from the middle part of the surface. These are the directions in the forward narrow cone near the axis of the spheroid. In this cone, the main components of the far field amplitude are the transverse components, while Ψ_z is asymptotically small.

We use the Cartesian components of the vectors, but perform the integration in the coordinates of the boundary layer, where

$$dS = bd\eta a\sqrt{1-\eta^2}d\varphi. \tag{55}$$

The unit vector along the η coordinate almost coincides with the unit vector along z, that is $J_z = J_\eta$ in the leading order, but the correction produces the J_r-component

$$J_r = -\frac{a}{b}\frac{\eta}{\sqrt{1-\eta^2}}J_\eta. \tag{56}$$

Using the fact that $J_\eta = H_\varphi$, $J_\varphi = -H_\eta$, and the expression

$$H_\eta = \frac{-i}{\sqrt{kb\chi\tau}\sqrt{1-\eta^2}}\left(2\tau\frac{\partial E_\varphi}{\partial\tau}+E_\varphi+\frac{\partial H_\varphi}{\partial\varphi}\right) \tag{57}$$

it is relatively straightforward to get

$$J_z = H_\varphi,\quad J_r = -\frac{a}{b}\frac{\eta}{\sqrt{1-\eta^2}}H_\varphi,\quad J_\varphi = \frac{i}{ka\sqrt{1-\eta^2}}\left(2\frac{\partial E_\varphi}{\partial\tau}-\frac{\partial H_\varphi}{\partial\varphi}\right). \tag{58}$$

Let us now consider the gradient of ψ. The differentiation by z at the leading order reduces to the multiplication by $-ik$ and the other derivatives can be expressed by the formulas

$$\frac{\partial\psi}{\partial x} = \frac{1}{a\sqrt{1-\eta^2}}\left(\left(2\frac{\partial\psi}{\partial\tau}-i\chi\eta\psi\right)\cos\varphi-\frac{\partial\psi}{\partial\varphi}\sin\varphi\right), \tag{59}$$

$$\frac{\partial\psi}{\partial y} = \frac{1}{a\sqrt{1-\eta^2}}\left(\left(2\frac{\partial\psi}{\partial\tau}-i\chi\eta\psi\right)\sin\varphi+\frac{\partial\psi}{\partial\varphi}\cos\varphi\right). \tag{60}$$

The substitution of the above expressions to the formula for $\mathbf{\Psi}$ yields

$$\Psi_x = -\frac{b}{4\pi}\int\limits_{-1}^{1}d\eta\int\limits_{0}^{2\pi}d\varphi\left\{\left(2\frac{\partial E_\varphi}{\partial\tau}-\frac{\partial H_\varphi}{\partial\varphi}\right)\psi\cos\varphi - H_\varphi\left(2\frac{\partial\psi}{\partial\tau}\sin\varphi+\frac{\partial\psi}{\partial\varphi}\cos\varphi\right)\right\}, \tag{61}$$

$$\Psi_y = -\frac{b}{4\pi}\int\limits_{-1}^{1}d\eta\int\limits_{0}^{2\pi}d\varphi\left\{\left(2\frac{\partial E_\varphi}{\partial\tau}-\frac{\partial H_\varphi}{\partial\varphi}\right)\psi\sin\varphi + H_\varphi\left(2\frac{\partial\psi}{\partial\tau}\cos\varphi-\frac{\partial\psi}{\partial\varphi}\sin\varphi\right)\right\}. \tag{62}$$

Next, we compute the integrals that express φ. The subintegral terms contain products of three trigonometric functions. Evidently the nonzero contributions are due to terms containing the products of three cosines, or two sines and one cosine with $|m-n|=1$. One can show that, in view of the symmetry of the problem, the following formulas hold:

$$\Psi_x^{\mathrm{TE}} = \sum_{n=0}^{+\infty} \Psi_{nx}^{\mathrm{TE}} \cos(n\varphi_0), \quad \Psi_y^{\mathrm{TE}} = \sum_{n=1}^{+\infty} \Psi_{ny}^{\mathrm{TE}} \sin(n\varphi_0), \tag{63}$$

$$\Psi_x^{\mathrm{TM}} = \sum_{n=1}^{+\infty} \Psi_{nx}^{\mathrm{TM}} \sin(n\varphi_0), \quad \Psi_y^{\mathrm{TM}} = \sum_{n=0}^{+\infty} \Psi_{ny}^{\mathrm{TM}} \cos(n\varphi_0). \tag{64}$$

For the harmonics we get

$$\Psi_{nx} = -\frac{b}{4}\int_{-1}^{1} \left\{ \psi_n \left(\frac{\partial}{\partial\tau}+\frac{1}{2}\right)(E_{n+1}+E_{n-1}) \pm (H_{n+1}-H_{n-1}) \left(\frac{\partial}{\partial\tau}+\frac{1}{2}\right)\psi_n \right\} d\eta, \tag{65}$$

$$\Psi_{ny} = -\frac{b}{4}\int_{-1}^{1} \left\{ \psi_n \left(\frac{\partial}{\partial\tau}+\frac{1}{2}\right)(E_{n+1}-E_{n-1}) \pm (H_{n+1}+H_{n-1}) \left(\frac{\partial}{\partial\tau}+\frac{1}{2}\right)\psi_n \right\} d\eta. \tag{66}$$

In the above, the plus signs are to be used for the TM incident wave and the minus signs for the TE case. The quantities E_n and H_n in (65) and (66) stand for the angular harmonics of E_φ and H_φ; the expressions for which can be deduced from (38) and (39). When substituting these expressions, the terms with the indexes $n-2$ and $n+2$ appear. These terms can be excluded by using the properties of the reflection coefficients. Further, we change the order of integration and use the formula

$$\int_{-1}^{1} \left(\frac{1-\eta}{1+\eta}\right)^{i(t-s)} \frac{d\eta}{1-\eta^2} = \pi\delta(t-s), \tag{67}$$

which reduces the integration by s and results in the compensation of the terms containing Whittaker functions $M_{it,n/2}(-i\chi)$. The Wronskians of Whittaker functions (42) are separated in the other terms, and we get

$$\begin{bmatrix} \Psi_{nx}^{\mathrm{TE}} \\ \Psi_{ny}^{\mathrm{TE}} \\ \Psi_{nx}^{\mathrm{TM}} \\ \Psi_{ny}^{\mathrm{TM}} \end{bmatrix} = \frac{ib(-1)^n}{\pi(n!)^3\beta\beta_0} \int_{-\infty}^{+\infty} \Gamma^2\left(\tfrac{n+1}{2}+it\right)\Gamma\left(\tfrac{n+1}{2}-it\right) M_{it,n/2}(i\beta^2) M_{it,n/2}\left(i\beta_0^2\right) \begin{bmatrix} -T_{n-1}^{\mathrm{TE}} - R_{n+1}^{\mathrm{TE}} \\ T_{n-1}^{\mathrm{TE}} - R_{n+1}^{\mathrm{TE}} \\ -T_{n-1}^{\mathrm{TM}} + R_{n+1}^{\mathrm{TM}} \\ T_{n-1}^{\mathrm{TM}} + R_{n+1}^{\mathrm{TM}} \end{bmatrix} dt, \tag{68}$$

In the above formulas, we have used the fact that $T_{-1}^{\mathrm{TE}} \equiv 0$ and $T_{-1}^{\mathrm{TM}} \equiv 0$.

Finally, we substitute the expressions for the reflection coefficients given by (40), (41), and (43), in (68), and rewrite Whittaker functions in terms of the Coulomb wave functions F and H^+ [16]. These cumbersome, though straightforward derivations result in the following expressions for the far field amplitudes of the magnetic vector:

$$\begin{bmatrix} \Psi_x^{\mathrm{TE}} \\ \Psi_y^{\mathrm{TE}} \end{bmatrix} = \frac{8ib}{\pi\beta\beta_0} \sum_{\ell=0}^{+\infty} \int_{-\infty}^{+\infty} \begin{bmatrix} (a_\ell^+ + b_\ell^+)\cos(\ell\varphi) \\ (a_\ell^+ - b_\ell^+)\sin(\ell\varphi) \end{bmatrix} dt, \tag{69}$$

$$\begin{bmatrix} \Psi_x^{\mathrm{TM}} \\ \Psi_y^{\mathrm{TM}} \end{bmatrix} = \frac{8ib}{\pi\beta\beta_0} \sum_{\ell=0}^{+\infty} \int_{-\infty}^{+\infty} \begin{bmatrix} (a_\ell^- + b_\ell^-)\sin(\ell\varphi) \\ (a_\ell^- - b_\ell^-)\cos(\ell\varphi) \end{bmatrix} dt. \tag{70}$$

Here

$$a_\ell^{\pm} = \frac{F_{\frac{\ell-1}{2}}\left(t, \frac{1}{2}\beta^2\right)}{z_\ell}\left(y_\ell F_{\frac{\ell-1}{2}}\left(t, \frac{1}{2}\beta_0^2\right) \pm F_{\frac{\ell+1}{2}}\left(t, \frac{1}{2}\beta_0^2\right)\right), \tag{71}$$

$$b_0^+ = 0, \quad b_1^+ = F_0\left(t, \frac{1}{2}\beta^2\right) F_0\left(t, \frac{1}{2}\beta_0^2\right) \frac{F_0\left(-t, \frac{1}{2}\chi\right)}{H_0^+\left(-t, \frac{1}{2}\chi\right)}, \tag{72}$$

$$b_0^- = 0, \quad b_1^- = F_0\left(t, \frac{1}{2}\beta^2\right) F_0\left(t, \frac{1}{2}\beta_0^2\right) \frac{\dot{F}_0\left(-t, \frac{1}{2}\chi\right)}{\dot{H}_0^+\left(-t, \frac{1}{2}\chi\right)}, \tag{73}$$

$$b_{\ell+2}^{\pm} = \frac{F_{\frac{\ell+1}{2}}\left(t, \frac{1}{2}\beta^2\right)}{z_\ell}\left(F_{\frac{\ell-1}{2}}\left(t, \frac{1}{2}\beta_0^2\right) \pm y_\ell F_{\frac{\ell+1}{2}}\left(t, \frac{1}{2}\beta_0^2\right)\right), \tag{74}$$

$$y_\ell = H_{\frac{\ell-1}{2}}^+\left(-t, \frac{1}{2}\chi\right) \dot{F}_{\frac{\ell+1}{2}}\left(-t, \frac{1}{2}\chi\right) + \dot{H}_{\frac{\ell-1}{2}}^+\left(-t, \frac{1}{2}\chi\right) F_{\frac{\ell+1}{2}}\left(-t, \frac{1}{2}\chi\right), \tag{75}$$

$$z_\ell = H_{\frac{\ell-1}{2}}^+\left(-t, \frac{1}{2}\chi\right) \dot{H}_{\frac{\ell+1}{2}}^+\left(-t, \frac{1}{2}\chi\right) + \dot{H}_{\frac{\ell-1}{2}}^+\left(-t, \frac{1}{2}\chi\right) H_{\frac{\ell+1}{2}}^+\left(-t, \frac{1}{2}\chi\right). \tag{76}$$

In the above formulas, the dots over F or H^+ denote the derivatives of the Coulomb wave functions with respect to their second argument. For the case of $\beta = 0$ or $\beta_0 = 0$, the representations (69), (69)

Table 2. Tests for RCS (in Db) for different frequencies f (in GHz).

Spheroid No. 1: $a = 0.5$, $b = 1.25$

f	χ	kb	RCS (asympt.)	RCS (ANSYS)	error (%)
0.1	0.419	2.620	−3.465522	−3.093652	12.0
0.5	2.096	13.099	13.563413	13.640915	−0.6
1.0	4.192	26.198	19.714119	19.709806	0.02
1.5	6.288	39.297	23.189528	23.133993	0.24
2.0	8.383	52.396	25.640673	25.534817	0.41
3.0	12.575	78.594	29.096819	28.866631	0.80
4.0	16.767	104.792	31.555742	31.119144	1.40

Spheroid No. 2: $a = 0.5$, $b = 1.77$

f	χ	kb	RCS (asympt.)	RCS (ANSYS)	error (%)
0.1	0.296	3.710	−4.778582	−4.666430	2.40
0.5	1.480	18.548	13.297679	13.350484	−0.4
1.0	2.960	37.096	19.698526	19.673893	0.13
1.5	4.440	55.645	23.232285	23.148338	0.36
2.0	5.920	74.193	25.697454	25.551617	0.57
3.0	8.881	111.289	29.152752	28.824957	1.13
4.0	11.841	148.386	31.604748	31.050392	1.78

Spheroid No. 3: $a = 0.3125$, $b = 1.39$

f	χ	kb	RCS (asympt.)	RCS (ANSYS)	error (%)
0.1	0.147	2.913	−16.194632	−16.029930	1.03
0.5	0.736	14.566	3.977269	4.044432	−1.66
1.0	1.472	29.132	11.148134	11.121439	0.24
1.5	2.209	43.698	14.966856	14.862905	0.70
2.0	2.945	58.264	17.553463	17.369444	1.05
3.0	4.417	87.397	21.088469	20.732029	1.72
4.0	5.890	116.529	23.554020	22.986029	2.47

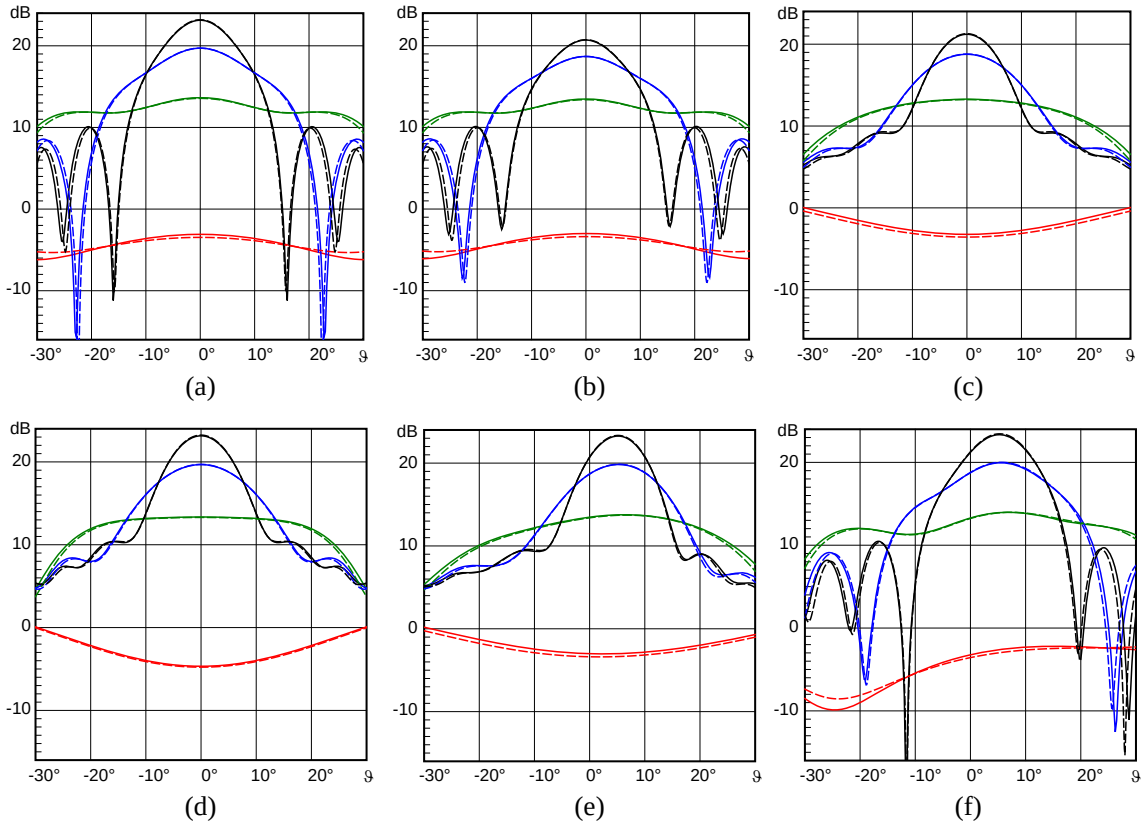

Figure 4. RCS for spheroid No. 1: (a), (d) for axially incident TE plane wave, (b), (e) for TE incident wave at 5° and for (c), (f) TM incident wave at 5°. The section by the plane $\varphi = 0°$ is given in (a), (b), (c) and the section at $\vartheta = 90°$ is in (d), (e), (f). Solid lines are for the results obtained by ANSYS, dashed lines present asymptotic results.

contain an ambiguity. When avoiding it, we take into account of the fact that

$$\frac{F_{-1/2}\left(t, \frac{1}{2}\beta^2\right)}{\beta} \to \sqrt{\frac{\pi/2}{e^{2\pi i t}+1}} \tag{77}$$

while Coulomb wave functions F_ℓ with other indices vanish.

Though Formulas (69) and (69) are rather cumbersome and contain infinite integration and summation, computational difficulties are mostly encountered in the computation of the Coulomb wave functions, but are effectively resolved by using the Fortran program developed in [18]. The integrals in Formulas (69), (69) exponentially converge at infinity. For the purpose of numerical computation, we discard the semi-infinite intervals for which the absolute value of the integrated function is more than a million times less than its maximum value. For the remaining interval, it is usually sufficient to choose the step of integration smaller than 0.4. To minimize the computational errors we use a step which is 10 times smaller; i.e., 0.04, which typically results in 150–300 integration nodes, less for smaller values of the elongation parameter χ and scaled angles β and β_0. The number of terms in the series depends on the parameters β and β_0, but it is usually sufficient to consider no more than 10 terms. We used 20 terms for the results presented below.

5. COMPARISON WITH NUMERICAL TESTS AND EFFECT OF STRONG ELONGATION

We validate the above asymptotic approach by comparing the RCS

$$\mathrm{RCS} = 4\pi \|\mathbf{\Psi}\|^2 \tag{78}$$

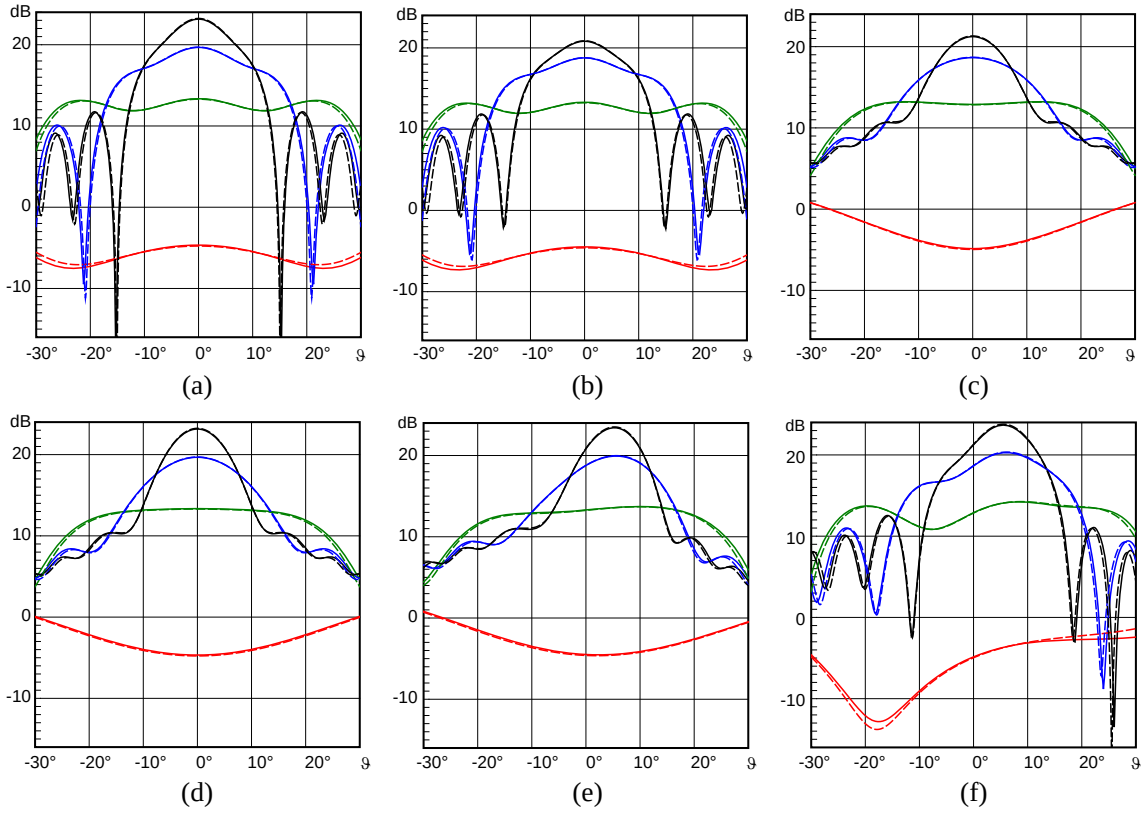

Figure 5. RCS for spheroid No. 2 (see caption of Figure 4).

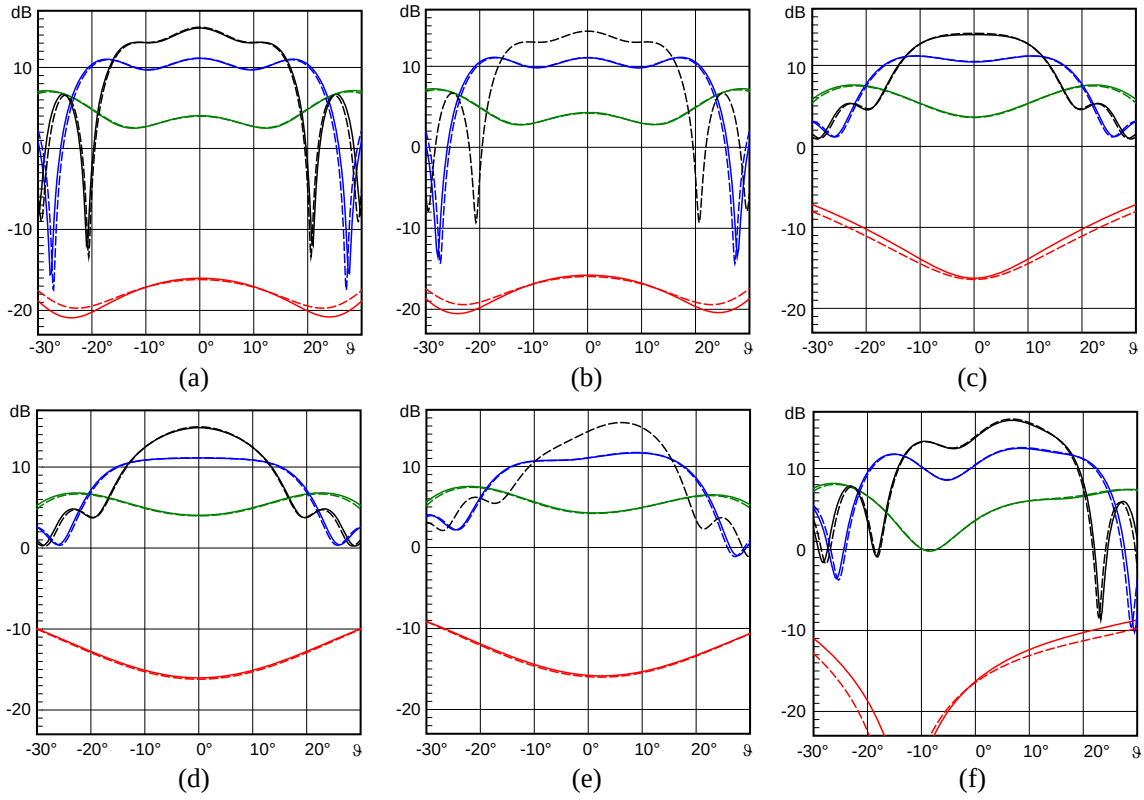

Figure 6. RCS for spheroid No. 3 (see caption of Figure 4).

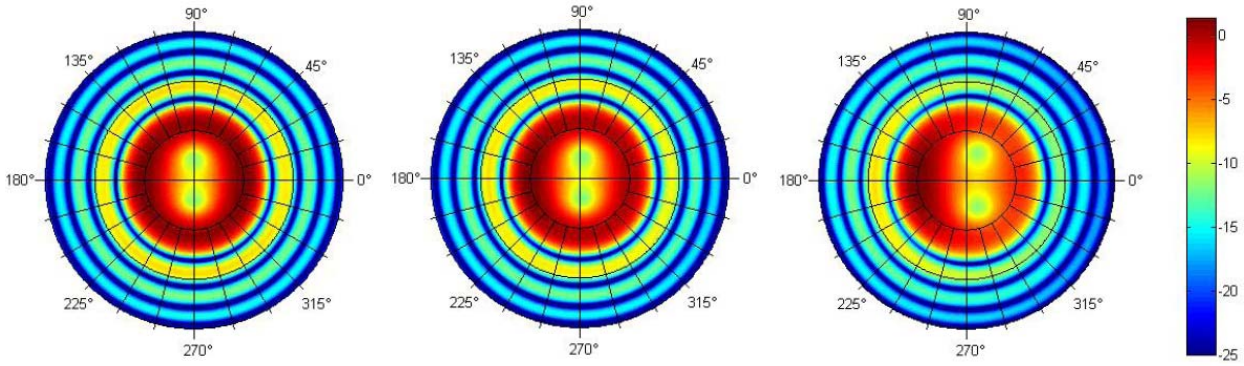

Figure 7. RCS of TE wave on the spheroid No. 4 for the incidence at 0, 1° and 5°.

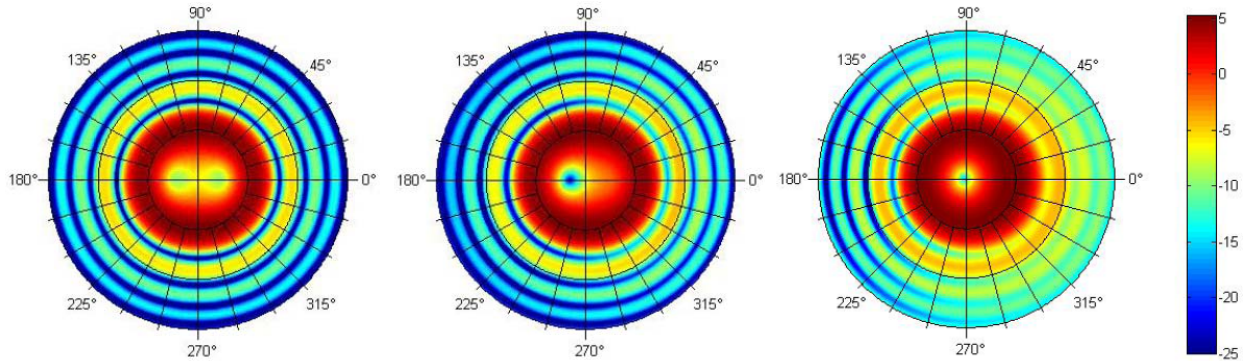

Figure 8. RCS of TM wave on the spheroid No. 4 for the incidence at 0, 1° and 5°.

computed by using (69) through (76), with those obtained by using the FEM/Boundary Element code HFSS from ANSYS[†]. For this purpose, we choose the same spheroids as above, but consider a larger set of frequencies, namely 100 MHz, 500 MHz, 1 GHz, 1.5 GHz, 2 GHz, 3 GHz and 4 GHz. The parameters of this comparison are listed in Table 2. We present in this table the values of the RCS on the axis for the case of axial incidence. It shows that the smallest difference between the asymptotic and numerical results for all three spheroids is achieved for 1 GHz frequency and corresponds to the values of the asymptotic parameter kb of about 26–37. For smaller values of the parameter kb, the asymptotics is less accurate. For larger, the difference is probably due to insufficient accuracy of numerical computations with ANSYS.

The RCS for different angles of observation are plotted in Figures 4 through 6. We consider in these figures the case of axial incidence and the case of incidence at an angle of 5° to the axis. Results for the frequency of 0.1 GHz are shown in red, for $f = 0.5$ GHz — in green, for 1 GHz in blue and for 1.5 GHz in black. We see that the agreement between the asymptotic and numerical results is at approximately the same level of accuracy as in Table 2 if the angles do not exceed 10°. For larger angles the agreement becomes less accurate, which is an expected result because when deriving the asymptotics we assumed the angles to be small.

Formulas (69) and (69) enable us to study the effect of strong elongation on the directivity of the scattered field. Figures 4 through 6 show that for moderately long spheroids, the main leaf of the RCS points to the direction of the incidence, and that there is no qualitative difference between the results for the TE and TM polarizations. For the case of spheroid No. 3, which is the most elongated, the main beam is not represented as well, though the maximum of the scattered field amplitude continues to point to approximate the direction of incidence.

For spheroids with larger elongations, the situation is significantly different and the influence of

[†] Computations were performed by D. Shevnin, CADFEM CIS Branch in North-West Federal Region. See also [24].

the polarization of the incident wave becomes more noticeable. Figures 7 and 8 present the RCS for the spheroid No. 4, with the semiaxes $b = 1\,\mathrm{m}$, $a = 5\,\mathrm{cm}$, at $5\,\mathrm{GHz}$. We observe that for axial incidence the maximum of the RCS is not located on the axis, but at approximately $\vartheta = 10^\circ$. Inside the cone formed by this maximum there are two directions in which the scattering amplitude has minima. For axial incidence these directions are on the opposite sides of the axis at about 5°. When the angle of incidence increases, some perturbations of these minima take place. For the TE case they both shift towards the direction of incidence and this decreases the RCS in that direction. As a result, we see the effect that the amplitude of the scattered field is more pronounced on the opposite side, as if the spheroid reflects the incident wave. For the TM case, one of the minima disappears when the angle of incidence increases from zero while the other shifts towards the axis.

6. CONCLUSION

In this paper, we have discussed the application of high-frequency asymptotic technique to solve the problem of diffraction by elongated bodies. We have shown that the classical asymptotic expansions provide reasonable approximations for such problems only if the asymptotic parameter is extremely large, which results in a possible gap between very large-scale problems, and moderately large problems for which numerical approaches are viable. The asymptotic representations derived under the supposition of a strongly elongated body enable us to close this gap. We have derived the approximations for both the induced currents and for the far field amplitude of the scattered field in the forward directions. These new formulas are uniform with respect to the elongation parameter χ. When this parameter increases to infinity, which can be achieved by setting the frequency very high, the formulas simplify to the classical asymptotic expressions. However, they remain applicable for moderately high frequencies, where the classical asymptotics fail.

In the frame of the presented approach, one can obtain asymptotic expansions for backward wave in the case of a skewed incidence on a strongly elongated body and for the back-scattering amplitude. This was done recently in [23] for the acoustic wave. One can also consider diffraction of spherical waves (for acoustics see [25]) or Gaussian beams. The approach is applicable also to some other canonical geometries [26] such as hyperboloids, cones [27], or elliptic cylinders [28].

More difficult extensions [29] would involve the implementation of the impedance boundary condition and application to geometries which do not possess a rotational symmetry.

REFERENCES

1. Fock, V. A., "The distribution of currents induced by a pane wave on the surface of a conductor," *Journ. of Phys. of the USSR*, Vol. 10, No. 2, 130–136, 1946.
2. Hönl, H., A. W. Maue, and K. Westpfahl, *Theorie der Beugung*, Springer-Verlag, Berlin-Göttingen-Heidelberg, 1961.
3. King, R. W. P. and T. T. Wu, *The Scattering and Diffraction of Waves*, Harward University Press, Cambridge, Massachusetts, 1959.
4. Belkina, M. G. and L. A. Wainstein, "The characteristics of radiation of spherical surface antennas," *Diffraction of Electromagnetic Waves by Some Bodies of Revolution*, 57–125, Sovetskoe Radio, Moscow, 1957 (in Russian).
5. Belkina, M. G., "The characteristics of radiation of a prolate ellipsoid of revolution," *Diffraction of Electromagnetic Waves by Some Bodies of Revolution*, 126–147, Sovetskoe Radio, Moscow, 1957 (in Russian).
6. Hong, S., "Asymptotic theory of electromagnetic and acoustic diffraction by smooth convex surfaces of variable curvature," *Journal of Mathematical Physics*, Vol. 8, No. 6, 1223–1232, 1967.
7. Ivanov, V. I., "Computation of corrections to the Fock asymptotics for the wave field near a circular cylinder and a sphere," *J. of Soviet Mathematics*, Vol. 20, No. 1, 1812–1817, 1982.
8. Andronov, I. V., D. P. Bouche, and M. Duruflé, "High-frequency diffraction of plane electromagnetic wave by an elongated spheroid," *IEEE Transactions on Antennas and Propag.*, Vol. 60, No. 11, 5286–5295, 2012.

9. Senior, T. B. A., "Disk scattering at edge-on incidence," *IEEE Transactions on Antennas and Propag.*, Vol. 17, No. 6, 751–756, 1969.
10. Senior, T. B. A., "Loop excitation of traveling waves," *Can. J. Phys.*, Vol. 40, 1736, 1962.
11. Bird, T. S., "Comparison of asymptotic solutions for the surface field excited by a magnetic dipole on a cylinder," *IEEE Transactions on Antennas and Propag.*, Vol. 32, No. 11, 1237–1244, 1984.
12. Andronov, I. V. and D. Bouche, "Asymptotic of creeping waves on a strongly prolate body," *Ann. Télécommun.*, Vol. 49, Nos. 3–4, 205–210, 1994.
13. Molinet, F., I. V. Andronov, and D. Bouche, *Asymptotic and Hybrid Methods in Electromagnetics*, IEE, London, 2005.
14. Engineer, J. C., J. R. King, and R. H. Tew, "Diffraction by slender bodies," *Eur. J. Appl. Math.*, Vol. 9, No. 2, 129–158, 1998.
15. Komarov, I. V., L. I. Ponomarev, and S. Y. Slavyanov, *Spheroidal and Coulomb Spheroidal Functions*, Nauka, Moscow, 1976 (in Russian).
16. Abramowitz, M. and I. Stegun, *Handbook of Mathematical Functions*, National Bureau of Standards, New York, 1964.
17. Andronov, I. V., "The currents induced by a high-frequency wave incident at a small angle to the axis of strongly elongated spheroid," *Progress In Electromagnetics Research M*, Vol. 28, 273–287, 2013.
18. Thompson, I. J. and A. R. Barnett, "COULCC: A continued-fraction algorithm for Coulomb functions of complex order with complex arguments," *Computer Physics Communications*, Vol. 36, 363–372, 1985.
19. Andronov, I. V. and D. Bouche, "Forward and backward waves in high-frequency diffraction by an elongated spheroid," *Progress In Electromagnetics Research B*, Vol. 29, 209–231, 2011.
20. Fock, V. A., *Electromagnetic Diffraction and Propagation Problems, (International Series of Monographs on Electromagnetic Waves)*, Chapter 3, Frankfurt, Pergamon Press, 1965.
21. Andronov, I. V., "High frequency asymptotics of electromagnetic field on a strongly elongated spheroid," *PIERS Online*, Vol. 5, No. 6, 536–540, 2009.
22. Stratton, J. A. and L. J. Chu, "Diffraction theory of electromagnetic waves," *Phys. Review*, Vol. 56, No. 1, 99–107, 1939.
23. Andronov, I. V., "High-frequency acoustic scattering from prolate spheroids with high aspect ratio," *Journal of the Acoustical Soc. Am.*, Vol. 134, No. 6, 4307–4316, 2013.
24. Andronov, I. V. and D. A. Shevnin, "High-frequency scattering by perfectly conducting prolate spheroids," *Journal of Electromagnetic Waves and Applications*, Vol. 28, No. 11, 1388–1396, 2014.
25. Andronov, I. V., "Diffraction of spherical waves on large strongly elongated spheroids," *Acta Acoustica United with Acoustica*, Vol. 99, No. 2, 177–182, 2013.
26. Andronov, I. V., "Calculation of diffraction by strongly elongated bodies of revolution," *Acoustical Physics*, Vol. 58, No. 1, 22–29, 2012.
27. Andronov, I. V. and D. Bouche, "Diffraction by a narrow circular cone as by a strongly elongated body," *Journal of Mathematical Sciences*, Vol. 185, No. 4, 517–522, 2012.
28. Andronov, I. V., "Diffraction by elliptic cylinder with strongly elongated cross-section," *Acoustical Physics*, Vol. 60, No. 3, 237–244, 2014.
29. Andronov, I. V. and R. Mittra, "Asymptotic theory of diffraction by elongated bodies — From V. A. Fock to present," *Forum for Electromagnetic Research Methods and Application Technologies (FERMAT)*, Vol. 2, 1–16, 2014.